arXiv:0811.0185v3 [cond-mat.stat-mech] 28 Jun 2009

Dynamics of curved interfaces

Carlos Escudero

Instituto de Ciencias Matemáticas, Consejo Superior de Investigaciones Científicas, C/ Serrano 123, 28006 Madrid, Spain

Abstract

Stochastic growth phenomena on curved interfaces are studied by means of stochastic partial differential equations. These are derived as counterparts of linear planar equations on a curved geometry after a reparametrization invariance principle has been applied. We examine differences and similarities with the classical planar equations. Some characteristic features are the loss of correlation through time and a particular behaviour of the average fluctuations. Dependence on the metric is also explored. The diffusive model that propagates correlations ballistically in the planar situation is particularly interesting, as this propagation becomes nonuniversal in the new regime.

PACS numbers: 68.35.Ct, 02.40.Ky, 05.40.-a, 68.35.Fx

I. INTRODUCTION

Growing interfaces appear everywhere in the natural world. Some of them are as important as the technologically motivated thin film deposition, medically relevant as bacterial colonies development, and physically interesting as fluid flow in porous media. Together with these, one finds a large variety of situations where the main driving mechanism is a growing fluctuating interface. Despite their diverse origin, all these phenomena have been studied within the common formalism of scaling analysis [1]. This theory classifies different growth phenomena into university classes, characterized by sets of critical exponents which encode information about the interface morphology and dynamics. In consequence, two different processes lying in the same universality class are supposed to have the same underlying physical mechanism driving the growth. This methodology has been successfully applied to a broad range of situations, but however, there are a number of restrictions that limit the traditional form of scaling analysis. One of them is the assumption that the interface can be described from a Cartesian reference frame, standard for planar surfaces. Another common assumption is the time independence of the substrate size. Despite the usefulness of the Cartesian representation in many cases, there are some growth profiles that can not be described according to it. Physical settings such as fluid flow in porous media [1], grain-grain displacement in Hele-Shaw cells [2], fracture dynamics [3], adatom and vacancy islands on crystal surfaces [4], and atomic ledges bordering crystalline facets [5, 6] present interfaces that violate the hypothesis of the Cartesian representation. Biological systems are also characterized by an approximate spherical symmetry: bacterial colonies [7], fungi [8], epithelial cells [9], and cauliflowers [10] develop rough surfaces which are not describable from a planar reference frame. Also, different contexts like the technological liquid composite molding [11], geological processes as stromatolite morphogenesis [12], and chemical structures [13] provide examples of interfaces that either become larger as time evolves or have a curved geometry, revealing the broad presence of this phenomenon in the natural world.

The theoretical study of non-equilibrium radial growth probably started with the seminal work of Eden [14], but the use of stochastic growth equations appeared only more recently, with the introduction of the Kardar-Parisi-Zhang (KPZ) equation in reparametrization invariant form [15]. Subsequent works were devoted to the radial $(1+1d)$ KPZ equation [16, 17, 18], the radial $(1+1d)$ and spherical $(2+1d)$ Mullins-Herring (MH) equa-

tion [19, 20], and the general reparametrization invariant formulation of stochastic growth equations [21]. An analytical approach to these equations [18] showed that for short spatial scales and time intervals the dynamics of radial interfaces was equivalent to that of the planar case; however, long time intervals yielded a different output. In a recent work these results have been expanded showing that for fast surface growth dilution acts as a dominant mechanism in the large scale [22], explaining the discrepancies in this limit. Dilution refers to the fact that the already deposited material becomes distributed in a larger area, and it thus gets diluted inside the material being deposited at the time. Herein we will limit ourselves to large spatial scale properties of solutions to equations whose planar counterparts are linear, and we will generalize our previous results [23]. The numerical study of the Eden model in [18] suggests that dilution is not taking place in this particular model; using this result as a benchmark we will phenomenologically neglect dilution in the equations under consideration.

The rest of the paper is organized as follows: in section II we study growing radial interfaces and section III is concerned with spherical interfaces; in both cases we consider a broader range of relaxation mechanisms than in the previous work [23]. Section IV is devoted to different geometries of physical interest, which are introduced in this work for the sake of completeness, and finally, in section V we draw our main conclusions and discuss possible lines for future research.

II. RADIAL GEOMETRY

The equation of growth of a general curved surface reads [21]

$$\partial_t \vec{r}(\mathbf{s},t) = \hat{n}(\mathbf{s},t)\Gamma[\vec{r}(\mathbf{s},t)] + \vec{\Phi}(\mathbf{s},t), \tag{1}$$

where the $d+1$ dimensional surface vector $\vec{r}(\mathbf{s},t) = \{r_\alpha(\mathbf{s},t)\}_{\alpha=1}^{d+1}$ runs over the surface as $\mathbf{s} = \{s^i\}_{i=1}^{d}$ varies in a parameter space. In this equation $\hat{n}$ stands for the unitary vector normal to the surface at $\vec{r}$, Γ contains a deterministic growth mechanism that causes growth along the normal $\hat{n}$ to the surface, and $\vec{\Phi}$ is a random force acting on the surface. The stochastic term acts on the normal direction too $\vec{\Phi} = \hat{n}\eta$, while the noise η is assumed to be a Gaussian variable with zero mean and correlation given by

$$\langle \eta(\mathbf{s},t)\eta(\mathbf{s}',t')\rangle = n_\alpha(\mathbf{s},t)n_\beta(\mathbf{s},t)\epsilon\Gamma^{\alpha\beta}g^{-1/2}\delta(\mathbf{s}-\mathbf{s}')\delta(t-t'), \tag{2}$$

where g denotes the metric tensor determinant and the Einstein summation convention has been adopted. The tensor $\Gamma^{\alpha\beta}$ specifies the geometric properties of the noise. In our case we will only consider isotropic noises, i. e. $\Gamma^{\alpha\beta} = \delta^{\alpha\beta}$, implying $n_\alpha(\mathbf{s},t)n_\beta(\mathbf{s},t)\delta^{\alpha\beta} = 1$. Anisotropic noises appear, for instance, when considering deposition from a collimated beam of particles [21].

For simplicity, let us start considering radial geometry, characterized by the position vector

$$\vec{r} = (r(\theta,t)\cos(\theta), r(\theta,t)\sin(\theta))\,. \tag{3}$$

Most of the two-dimensional examples mentioned at the introduction belong to this class: adatom and vacancy islands on crystal surfaces, bacterial colonies, fungi, ... The shape of radial interfaces was illustrated by means of numerical simulations in [16] and [17]; their deterministic evolution is analogous to that of an elliptic interface of null eccentricity, see Sec. IV and Fig. 3. The effect of stochasticity in this $1+1d$ system was estimated logarithmic on average [23]. This result was obtained by means of a small noise expansion of the radial random deposition equation at first order in the fluctuation intensity. Of course, small noise expansions are appropriate only for limited times, as the unbounded nature of the Gaussian noise makes them invalid for arbitrary long times, for which the probability of rare events is not negligible. However, in our particular cases, this type of expansions yields reasonable results, as we will show. We will perform now a more detailed analysis of this phenomenon using Edwards-Wilkinson (EW) dynamics. The radial EW equation is the following Itô equation [16, 17, 23]

$$\partial_t r = \frac{D}{r^2}\partial_\theta^2 r - \frac{D}{r} + F + \frac{1}{\sqrt{r}}\eta(\theta,t), \tag{4}$$

where $\eta(\theta,t)$ is a zero mean Gaussian noise whose correlation is given by

$$\langle \eta(\theta,t)\eta(\theta',t')\rangle = \epsilon\delta(\theta-\theta')\delta(t-t'). \tag{5}$$

Using now the second order small noise expansion [24]

$$r(\theta,t) = R(t) + \sqrt{\epsilon}\rho_1(\theta,t) + \epsilon\rho_2(\theta,t), \tag{6}$$

yields

$$\frac{dR}{dt} = F - \frac{D}{R}, \tag{7}$$

$$\partial_t \rho_1 = \frac{D}{R^2}\left(\partial_\theta^2 \rho_1 + \rho_1\right) + \frac{1}{\sqrt{R}}\xi(\theta, t), \tag{8}$$

$$\partial_t \rho_2 = \frac{D}{R^2}\left(\partial_\theta^2 \rho_2 - \frac{2}{R}\rho_1 \partial_\theta^2 \rho_1 + \rho_2\right) - \frac{\rho_1}{2R^{3/2}}\xi(\theta, t), \tag{9}$$

where

$$\langle \xi(\theta, t)\xi(\theta', t')\rangle = \delta(\theta - \theta')\delta(t - t'). \tag{10}$$

One can see that the fluctuations present in the system in the large scale come from the ρ_1 dynamics. The reason is that the noise sources in the ρ_2 equation are subdominant. This can be seen by deriving the equation for the correlation $\langle \rho_2(\theta, t)\rho_2(\theta', t')\rangle$. The most stochastic term appearing in the resulting equation is proportional to the four points function

$$\langle \rho_1(\theta, t)\rho_1(\theta', t')\xi(\theta, t)\xi(\theta', t')\rangle = \langle \rho_1(\theta, t)\rho_1(\theta', t')\rangle \langle \xi(\theta, t)\xi(\theta', t')\rangle , \tag{11}$$

where the equality holds because the other products of two points functions vanish due to the noise interpretation. This is a consequence of the Itô interpretation in Eq. (4), which implies $\langle r\eta\rangle = \langle r\rangle\langle\eta\rangle$. Since we are decomposing the solution in the small noise expansion (6) the statistical independence among the solution and the noise holds at every order. We know the value of the correlator [23]

$$\langle \rho_1(\theta, t)\rho_1(\theta', t)\rangle = \frac{\delta(\theta - \theta')}{2\pi F}\ln(t), \tag{12}$$

which increases as the logarithm of time. As the four points function is multiplied by $R^{-3}(t) = (Ft)^{-3}$, this is equivalent to have the noise term damped as in the two dimensional situation (see [23] and Sec. III), making it subdominant, and the ρ_1 random variable divided by $\sqrt{t}$. The amplitude of this random variable increases as the square root of the logarithm of time, so this ratio vanishes in the long time limit too. The rest of the stochastic terms in the equation for the correlation $\langle \rho_2(\theta, t)\rho_2(\theta', t')\rangle$ either vanish due to the noise interpretation or have logarithmic amplitudes. As all these terms are multiplied by a negative power of the temporal variable they vanish in the long time limit, just like the terms we have considered here. This implies that the noise terms only contribute to create some constant prefactor, like in higher dimensional radial equations [23]. This remains true for all higher orders in the small noise expansion, so we can conclude that the stochasticity present in the system

comes from either the perturbation ρ_1 or non-analytic effects. To estimate the effect of these exponentially infrequent events we make use of large deviation theory in appendix A, where we show evidence pointing to their irrelevance using the radial random deposition equation. So combining these results suggests that the stochasticity present in the system comes from the first order term in the small noise expansion. Of course, this result is not rigorous, but indicates that only a very slow process can modify it. Taking into account the explicit temporal dependence in the equations for the stochastic perturbations it is clear that this type of process will be more and more infrequent as time evolves. In the hydrodynamic limit, the probability of observing such a rare event will be negligible for evolution times of interest. This will simplify the forthcoming analyses. Note that the present situation is completely different to that of the KPZ or other nonlinear planar stochastic growth equations. For them the small noise expansion is only valid for short times, but higher order corrections in this expansion or a WKB analysis show the measurable effect that small fluctuations have on the dynamics; contrarily, these sorts of analysis have shown negligible corrections in the current case, as we have shown in this section and in appendix A.

Before moving to different dynamics, let us clarify some properties of the radial EW equation. When we talk about the irrelevance of the infrequent events we refer to the behavior in the hydrodynamic limit, characterized by $t \to \infty$. For small sizes of the cluster, stochastic dynamics might be affected by the fixed point of Eq. (7), that separates the shrinking and the expanding tendencies [23]. In this regime, rare events might promote changes among these two types of evolution. In the long time limit and large spatial scale, however, radial EW dynamics reduces to radial random deposition [23], and thus infrequent events become irrelevant, in agreement with the results reported in appendix A. The exact solution of Eq. (7) and a study of its dynamics is reported in [23] and in Sec. III, and the analysis of the radial EW equation metastability properties is performed in [16] and in appendix B.

It is easy to generalize the EW equation to fractional orders in the planar case [25]

$$\partial_t h = D_\varsigma \Lambda^\varsigma h + \eta(x,t), \tag{13}$$

where $\Lambda^\varsigma h$ denotes a Riesz derivative, and its action on the function height $h(x,t)$ is defined by means of its Fourier transform

$$\widehat{\Lambda^\varsigma h} = -|k|^\varsigma \hat{h}(k,t), \tag{14}$$

where k denotes the Fourier variable. The case $\zeta = 2$ corresponds to the EW equation. The object of introducing these equations is twofold. On one hand they allow understanding the interplay of the value of exponent ζ, which specifies the velocity at which correlations propagate, and the other characteristics of the system. On the other hand, these fractional operators are common models describing anomalous transport properties of complex systems [26]. In this sense, one can think of fractional equations as physical generalizations of the classical Laplacian diffusion. It is not so straightforward however to obtain these equations in a general manifold. Let us recall the Beltrami-Laplace operator in one dimension

$$\Delta_{BL}\vec{r} = \frac{1}{\sqrt{g}}\partial_s\left(\frac{1}{\sqrt{g}}\partial_s\vec{r}\right), \tag{15}$$

where s parameterizes the corresponding manifold. Its structure suggests us a possible definition of "square-root" of this operator as

$$\tilde{\Lambda}\vec{r} = \frac{1}{\sqrt{g}}\Lambda_s\vec{r}, \tag{16}$$

where Λ_s is some derivative with the desired properties. Due to the intrinsic nonlinearity of this operator, we cannot define a fractional derivative along the lines of the Riesz one, because it takes advantage of the linearity of the ordinary derivative in order to use the Fourier transform. Nevertheless, we can generalize the radial EW equation to fractional orders assuming $r(\theta,t) = R(t) + \sqrt{\epsilon}\rho(\theta,t)$, $R(t) = Ft$, and the perturbation obeying the equation

$$\partial_t\rho = \frac{D_\zeta}{(Ft)^\zeta}\Lambda_\theta^\zeta\rho + \frac{1}{\sqrt{Ft}}\xi(\theta,t), \tag{17}$$

in the interval $[0, 2\pi]$, where the solution is subject to periodic boundary conditions. This equation, in the long time limit, coincides with the corresponding EW one when $\zeta = 2$, except for one term coming from the nonlinear dynamics of the curved surface, see Eq. (8). So this toy model retains part of the properties of the equation of motion for the interface, but part of the curvature effects is lost, and these are the cause of some stability deterioration as have been seen [17, 23]. However, we will see that the correlation obtained with this model is the same that the one obtained from the original equation for the perturbation. The correlation can be computed in terms of the Fourier transformed field

$\rho_n(t) = (2\pi)^{-1}\int_0^{2\pi}\rho(\theta,t)\exp(-in\theta)d\theta$:

$$\langle\rho_n(t)\rho_m(t)\rangle = \exp\left[\frac{D_\zeta(|m|^\zeta+|n|^\zeta)}{F^\zeta t^{\zeta-1}(\zeta-1)}\right]\left\{\exp\left[\frac{D_\zeta(|m|^\zeta+|n|^\zeta)}{F^\zeta t_0^{\zeta-1}(1-\zeta)}\right]\langle\rho_n(t_0)\rho_m(t_0)\rangle + \frac{\delta_{n,-m}}{2\pi F(\zeta-1)}\left(\mathrm{Ei}\left[\frac{D_\zeta(|m|^\zeta+|n|^\zeta)}{F^\zeta t_0^{\zeta-1}(1-\zeta)}\right]-\mathrm{Ei}\left[\frac{D_\zeta(|m|^\zeta+|n|^\zeta)}{F^\zeta t^{\zeta-1}(1-\zeta)}\right]\right)\right\}, \quad (18)$$

if $\zeta\neq 1$ (note that for $\zeta=2$ the result is the same as for the full radial EW equation [23]); here $n,m\in\mathbb{Z}$, $\mathrm{Ei}(x)=\int_{-\infty}^{x}t^{-1}e^t dt$ denotes the exponential integral [27], and this last integral has to be interpreted in terms of the Cauchy principal value when necessary. Using the asymptotic expansion $\mathrm{Ei}(x)\sim\ln(|x|)$ when $x\sim 0$ we find, when $\zeta>1$ and in the limit $t\to\infty$, that the correlation adopts the form

$$\langle\rho_n(t)\rho_m(t)\rangle\sim\frac{\delta_{n,-m}}{2\pi F}\ln(t), \qquad C(\theta,\theta',t)=\langle\rho(\theta,t)\rho(\theta',t)\rangle\sim\frac{\ln(t)}{2\pi F}\delta(\theta-\theta'), \quad (19)$$

and so reduces to radial random deposition, this is, becomes totally uncorrelated. If $\zeta<1$, and in the long time limit, we find that the correlation vanishes

$$\langle\rho_n(t)\rho_m(t)\rangle\to 0, \quad (20)$$

by means of the asymptotic expansion $\mathrm{Ei}(x)\sim e^x/x$ when $x\to\pm\infty$, and the resulting interface is flat. If $\zeta=1$, what we call the ballistic model, the correlation is

$$C(\theta,\theta',t)=\frac{1}{2\pi}\int_0^\tau\sum_{n=-\infty}^{\infty}e^{2|n|D_1(s-\tau)+in(\theta-\theta')}ds = \frac{1}{2\pi}\int_0^\tau\frac{\sinh[2D_1(\tau-s)]}{\cosh[2D_1(\tau-s)]-\cos(\theta-\theta')}ds\sim\frac{1}{2\pi F}\ln\left(\frac{t}{|\theta-\theta'|^{F/D_1}}\right), \quad (21)$$

where $\tau=\ln(t)/F$. The final expression has been obtained in the limit of long times and small angular differences. This result allows us to define the local dynamical exponent $z_{loc}=F/D_1$, which depends continuously on the ratio of the parameters F and D_1, and it is thus nonuniversal. The planar ballistic model is analyzed in appendix C, where it is shown that the correlations in this case propagate indeed ballistically, this is $z=1$ is the universal dynamical exponent.

The radial MH equation reads [19, 20]

$$\partial_t r=-\frac{K}{r^4}(\partial_\theta^2 r+\partial_\theta^4 r)+F+\frac{1}{\sqrt{r}}\eta(\theta,t). \quad (22)$$

It appeared due to its possible connection to tumor growth [19]. By means of a small noise expansion we find at the deterministic level, compare to Eq. (7), $R(t) = Ft$, while for the stochastic perturbation, compare to Eq. (8), we get

$$\partial_t \rho = -\frac{K}{F^4 t^4}(\partial_\theta^2 \rho + \partial_\theta^4 \rho) + \frac{1}{\sqrt{Ft}}\eta(\theta, t). \tag{23}$$

The Fourier transformed field obeys the equation

$$\frac{d\rho_n}{dt} = \frac{K}{F^4 t^4}(n^2 - n^4)\rho_n + \frac{1}{\sqrt{Ft}}\eta_n(t), \tag{24}$$

that yields the mean value

$$\langle \rho_n(t) \rangle = \langle \rho_n(t_0) \rangle \exp\left[\frac{K(n^2 - n^4)}{3F^4}\left(\frac{1}{t_0^3} - \frac{1}{t^3}\right)\right], \tag{25}$$

showing that all the modes are stable except $n = 0, \pm 1$, which are marginal, a situation reminiscent to that of the EW equation. The equation for the correlation $C_{n,m}(t) = \langle \rho_n(t)\rho_m(t) \rangle$

$$\frac{dC_{n,m}}{dt} = \frac{K(n^2 + m^2 - n^4 - m^4)}{F^4 t^4} C_{n,m} + \frac{\delta_{n,-m}}{2\pi F t}, \tag{26}$$

can be solved to get

$$\begin{aligned} C_{n,m}(t) = \exp\left[\frac{K(n^2 + m^2 - n^4 - m^4)}{3F^4}\left(\frac{1}{t_0^3} - \frac{1}{t^3}\right)\right] \times \\ \left[C_{n,m}(t_0) + \frac{\delta_{n,-m}}{6\pi F}\exp\left[\frac{K(-n^2 - m^2 + n^4 + m^4)}{3F^4 t_0^3}\right] \times \right. \\ \left.\left(\mathrm{Ei}\left[\frac{K(n^2 + m^2 - n^4 - m^4)}{3F^4 t_0^3}\right] - \mathrm{Ei}\left[\frac{K(n^2 + m^2 - n^4 - m^4)}{3F^4 t^3}\right]\right)\right]. \end{aligned} \tag{27}$$

Assuming an uncorrelated initial condition and using the asymptotic equivalence $\mathrm{Ei}(x) \sim \ln(|x|)$ when $x \sim 0$ yields

$$\langle \rho_n(t)\rho_m(t) \rangle \sim \frac{\delta_{n,-m}}{2\pi F}\ln(t), \qquad C(\theta, \theta', t) \sim \frac{\ln(t)}{2\pi F}\delta(\theta - \theta'), \tag{28}$$

when $t \to \infty$. We have found that in this case again, as happened with all the models such that $z > 1$, the interface becomes uncorrelated in the long time limit.

In order to unify the different equations let us build a generic one assuming that the drift comes from a potential

$$\Gamma[\vec{r}(s,t)] = -\frac{1}{\sqrt{g(s)}}\frac{\delta \mathcal{V}[\vec{r}(s,t)]}{\delta \vec{r}(s,t)}, \tag{29}$$

and this potential can be expanded in a power series of the surface mean curvature H

$$\mathcal{V} = \int d^d s \sqrt{g} \sum_{i=0}^{N} K_i H^i = \sum_{i=0}^{N} \mathcal{V}_i. \tag{30}$$

The general contribution to the drift then reads

$$\Gamma_i = -\frac{1}{\sqrt{g}} \hat{n} \cdot \frac{\delta \mathcal{V}_i}{\delta \vec{r}} = K_i \left(H^{i+1} - i\Delta_{BL} H^{i-1} - iH^{i-1} \sum_{j=1}^{d} \lambda_j^2 \right), \tag{31}$$

where λ_j are the eigenvalues of the matrix of the coefficients of the second fundamental form and express the principal curvatures of the surface. Applying this theory to the present case of radial growth we get an equation generalizing both EW and MH

$$\partial_t r = K_0 \left(\frac{\partial_\theta^2 r}{r^2} - \frac{1}{r} \right) + K_2 \left(\frac{1}{r^3} - 7\frac{\partial_\theta^4 r}{r^4} \right) + F + \frac{1}{\sqrt{r}} \eta(\theta, t), \tag{32}$$

where we have linearized the resulting equation in the different derivatives of r about zero (limit of small variations of the radius with respect to the angle) and have truncated the expansion at order two; note that this procedure left us with the EW (zeroth order, proportional to K_0) and MH-like (second order, proportional to K_2) terms, while the first order term vanishes identically (a different situation arises in higher dimensions, see section III). This equation is particularly interesting for its stability properties. The usual small noise expansion leaves us with a system of equations for the different Fourier modes, whose mean value is

$$\langle \rho_m(t) \rangle = \exp \left\{ -\frac{(t - t_0)[3F^2 K_0 (m^2 - 1) t^2 t_0^2 + K_2 (3 + 7m^4)(t^2 + t t_0 + t_0^2)]}{3F^4 t^3 t_0^3} \right\} \langle \rho_m(t_0) \rangle , \tag{33}$$

revealing that the modes $m = \pm 1, \pm 2, ...$ are stable and thus improving the stability of both EW and MH equations, for which the modes $m = \pm 1$ were only marginal [23]. The stochastic properties of this equation are also attractive from a metastability point of view, see appendix B, what suggests it is a reliable model for describing radial growth processes.

III. SPHERICAL GEOMETRY

In this section we concentrate on spherical $(2 + 1d)$ growth models. These models can appear when considering tumor growth [19] or other biological structures, or diffusing voids

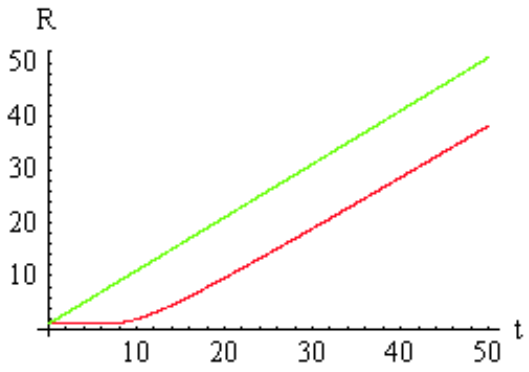


FIG. 1: Deterministic growth of the spherical cluster at zeroth order in the small noise expansion, see Eq. (36) in the main text, with parameter values $F = 1$, $K_0 = 1/2$, and $t_0 = 1 + 10^{-4}$ (red lower line). The linear law $t + 1 + 10^{-4}$ is plotted for comparison (green upper line).

inside a solid [28]. We will analyze the basic properties of the simplest equations that arise in this geometry using the position vector

$$\vec{r} = (r(\theta,\phi,t)\cos(\phi)\sin(\theta), r(\theta,\phi,t)\sin(\theta)\sin(\phi), r(\theta,\phi,t)\cos(\theta)). \tag{34}$$

The spherical EW equation reads

$$\partial_t r = K_0\left[\frac{\partial_\theta r}{r^2\tan(\theta)} + \frac{\partial_\theta^2 r}{r^2} + \frac{\partial_\phi^2 r}{r^2\sin^2(\theta)} - \frac{2}{r}\right] + F + \frac{1}{r\sqrt{\sin(\theta)}}\eta(\theta,\phi,t). \tag{35}$$

Note that its drift is proportional to the mean curvature of the interface $\Gamma = K_0 H$, once the small gradient expansion has been performed. As usual, we will decompose the solution into a deterministic radial part and a small stochastic perturbation $r(t) = R(t) + \epsilon\rho(\theta,t)$. The deterministic part obeys an equation that is analogous to the one obeyed by its $1+1d$ counterpart $\dot{R} = F - 2K_0R^{-1}$, see Eq. (7), and that can be solved to yield [23]

$$R(t) = \frac{2K_0}{F}\left\{1 + \mathcal{W}_0\left[\left(\frac{F^2t_0}{2K_0} - 1\right)\exp\left(\frac{F^2t}{2K_0} - 1\right)\right]\right\}, \tag{36}$$

where the initial condition was assumed to be $R(t_0) = Ft_0$, and it behaves asymptotically in time as $R(t) \sim Ft$ when $F^2t_0 > 2K_0$, see Fig. 1; if this inequality is reversed then the solution shrinks till it collapses in finite time [23], see Fig. 2. Here $\mathcal{W}_0$ denotes the principal branch of the Lambert omega function [29]. The random perturbation obeys the equation

$$\partial_t\rho = \frac{K_0}{F^2t^2}\left[\frac{\partial_\theta\rho}{\tan(\theta)} + \partial_\theta^2\rho + \frac{\partial_\phi^2\rho}{\sin^2(\theta)} + 2\rho\right] + \frac{1}{Ft\sqrt{\sin(\theta)}}\eta(\theta,\phi,t). \tag{37}$$

Now we assume that the solution can be decomposed as a linear combination of the spherical harmonics

$$\rho(\theta,\phi,t)=\sum_{l=0}^{\infty}\sum_{m=-l}^{l}\rho_l^m(t)Y_l^m(\theta,\phi). \tag{38}$$

The linearity of Eq. (37) allows us to write the evolution equation for the different modes

$$\frac{d\rho_l^m}{dt}=\frac{K_0}{F^2t^2}[2-l(l+1)]\rho_l^m+\frac{\eta_l^m(t)}{Ft}, \tag{39}$$

where the spherical noise has been expanded in spherical harmonics as well

$$\frac{\eta(\theta,\phi,t)}{\sqrt{\sin\theta}}=\sum_{l=0}^{\infty}\sum_{m=-l}^{l}\eta_l^m(t)Y_l^m(\theta,\phi), \tag{40}$$

and $\eta_l^m(t)$ is a zero mean Gaussian distributed random process, whose correlation reads

$$\left\langle \eta_l^m(t)\eta_{l'}^{m'}(t')\right\rangle=(-1)^m\delta_{m,-m'}\delta_{l,l'}\delta(t-t'). \tag{41}$$

Note that the presence of the Condon-Shortley phase in the correlation makes the noise change from real to imaginary and back as we vary m. We can solve Eq. (39) for its mean value

$$\langle\rho_l^m(t)\rangle=\exp\left[-\frac{K_0(l^2+l-2)(t-t_0)}{F^2tt_0}\right]\langle\rho_l^m(t_0)\rangle\,, \tag{42}$$

which is independent of the value of m except for the initial condition, and shows the linear stability of the spherical symmetric phase for the values $l>1$. Perturbations with $l=0$ are unstable, while $l=1$ characterizes the marginal case, a situation reminiscent to that of $1+1$ dimensional radial growth [23]. Its correlation function $C_{l,l'}^{m,m'}(t)=\left\langle\rho_l^m(t)\rho_{l'}^{m'}(t)\right\rangle$ obeys the differential equation

$$\frac{dC_{l,l'}^{m,m'}}{dt}=\frac{K_0[4-l(l+1)-l'(l'+1)]}{F^2t^2}C_{l,l'}^{m,m'}+\frac{(-1)^m\delta_{m,-m'}\delta_{l,l'}}{F^2t^2}, \tag{43}$$

that can be solved to yield

$$\begin{aligned}C_{l,l'}^{m,m'}(t)=C_{l,l'}^{m,m'}(t_0)\exp\left[-\frac{K_0[l(l+1)+l'(l'+1)-4](t-t_0)}{F^2tt_0}\right]\\ +\frac{1-\exp\left[-\frac{K_0[l(l+1)+l'(l'+1)-4](t-t_0)}{F^2tt_0}\right]}{K_0[l(l+1)+l'(l'+1)-4]}(-1)^m\delta_{m,-m'}\delta_{l,l'}.\end{aligned} \tag{44}$$

The correlation is bounded as $t\to\infty$, and it is a function of t_0. If we now take the limit $t_0\to\infty$ we find

$$\lim_{t_0\to\infty}\lim_{t\to\infty}C_{l,l'}^{m,m'}(t)=0. \tag{45}$$

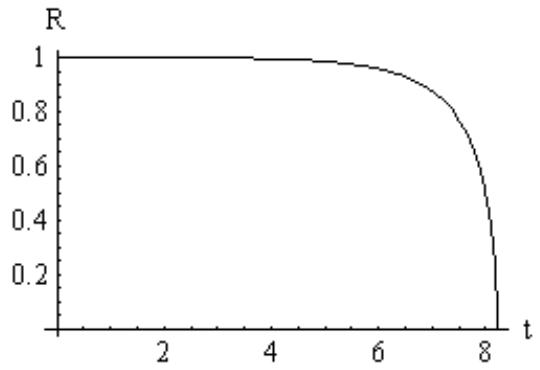


FIG. 2: Deterministic collapse of the spherical cluster at zeroth order in the small noise expansion, see Eq. (36) in the main text, with parameter values $F = 1$, $K_0 = 1/2$, and $t_0 = 1 - 10^{-4}$.

This means that fluctuations average out in the limit we are considering. The physical reason is that the surface area continuously grows while the parameter space stays constant. However, the surface might accumulate some average roughness produced by perturbations in earlier stages of growth. This finite size effect reflects the memory of the growth process with respect to the time the perturbation was set in. This is a consequence of the existence of an absolute origin of time in this system: the instant characterized by a cluster with zero radius. As the temporal and spatial scales of this system are intimately related, the hydrodynamic limit is characterized by an infinite lapse of time from the absolute temporal origin. Interestingly, perturbations happening at the first stages still remain in the interface in this limit; however, perturbations starting later have no effect on the average dynamics. We have shown elsewhere that this effect is a consequence of the absence of dilution and a fast radius growth [22].

If we perform an expansion from a potential in a power series of the mean curvature, just like at the end of section II, we will find again the spherical EW equation at zeroth order, but in this case the first order does not vanish. If we use this first order as the drift of a full stochastic growth equation we obtain what we call the intrinsically spherical (IS) equation

$$\partial_t r = K_1 \left[\frac{\partial_\theta^2 r}{r^3} + \frac{\partial_\phi^2 r}{r^3 \sin^2(\theta)} + \frac{\partial_\theta r}{r^3 \tan(\theta)} - \frac{1}{r^2} \right] + F + \frac{1}{r\sqrt{\sin(\theta)}} \eta(\theta, \phi, t), \tag{46}$$

that has no $1+1$ dimensional analog. We proceed to analyze this equation as usual. The solution of the spherical symmetric equation $\dot{R} = F - K_1 R^{-2}$ can be obtained in implicit

form

$$R(t) - \sqrt{\frac{K_1}{F}}\text{arctanh}\left[\sqrt{\frac{F}{K_1}}R(t)\right] = Ft - \sqrt{\frac{K_1}{F}}\text{arctanh}\left[\frac{F^{3/2}t_0}{\sqrt{K_1}}\right]. \tag{47}$$

The solution grows unboundedly for initial conditions such that $F^{3/2}t_0 > K_1^{1/2}$, and it adopts the linear growth $R \sim Ft$ in the long time limit; when this inequality is reversed then the solution shrinks till it collapses in finite time. The equation for the stochastic perturbation reads this time

$$\partial_t \rho = \frac{K_0}{F^3 t^3}\left[\frac{\partial_\theta \rho}{\tan(\theta)} + \partial_\theta^2 \rho + \frac{\partial_\phi^2 \rho}{\sin^2(\theta)} + 2\rho\right] + \frac{1}{Ft\sqrt{\sin(\theta)}}\eta(\theta,\phi,t). \tag{48}$$

The spherical harmonics decomposition yields for the mean value of the perturbation

$$\langle \rho_l^m(t)\rangle = \exp\left[-\frac{K_1(l^2+l-2)(t^2-t_0^2)}{2F^3 t^2 t_0^2}\right]\langle \rho_l^m(t_0)\rangle, \tag{49}$$

what reveals that the mode $l = 0$ is unstable, the modes with $l = 1$ are marginal, and the rest of the modes is stable, exactly the same as for the spherical Edwards-Wilkinson equation. For the correlation function we get

$$\begin{aligned} C_{l,l'}^{m,m'}(t) = \exp\left[\frac{K_1[l(l+1)+l'(l'+1)-4]}{2F^3}(t^{-2}-t_0^{-2})\right] C_{l,l'}^{m,m'}(t_0) \\ +(-1)^m \delta_{m,-m'}\delta_{l,l'}\sqrt{\frac{2}{FK_1[4-l(l+1)-l'(l'+1)]}}\times \\ \left\{\exp\left[\frac{K_1[l(l+1)+l'(l'+1)-4]}{2F^3}(t^{-2}-t_0^{-2})\right]\times \right. \\ \mathcal{D}\left[\sqrt{\frac{K_1[4-l(l+1)-l'(l'+1)]}{2F^3}}t_0^{-1}\right] \\ \left. -\mathcal{D}\left[\sqrt{\frac{K_1[4-l(l+1)-l'(l'+1)]}{2F^3}}t^{-1}\right]\right\}, \end{aligned} \tag{50}$$

where $\mathcal{D}(x) = e^{-x^2}\int_0^x e^{y^2}dy$ is the Dawson integral [27]. Using the fact that $\mathcal{D}(x) \sim x$ when $x \sim 0$, we can deduce that the correlation is bounded as $t \to \infty$, and we also recover the same result, Eq.(45), as in the last case.

The spherical Mullins-Herring equation reads [19, 20]

$$\begin{aligned} \partial_t r = -\frac{K_2}{r^4}\left\{[2+\sin^{-2}(\theta)]\tan^{-1}(\theta)\partial_\theta r - \tan^{-2}(\theta)\partial_\theta^2 r + 2\tan^{-1}(\theta)\partial_\theta^3 r + \partial_\theta^4 r \right. \\ \left. -2\sin^{-2}(\theta)\tan^{-1}(\theta)\partial_\phi^2\partial_\theta r + 2\sin^{-2}(\theta)\partial_\phi^2\partial_\theta^2 r + \sin^{-4}(\theta)[4\partial_\phi^2 r + \partial_\phi^4 r]\right\} \\ +F + \frac{1}{r\sqrt{\sin(\theta)}}\eta(\theta,\phi,t). \end{aligned} \tag{51}$$

It appears when surface diffusion occurs to minimize the surface area, yielding the drift term $\Gamma = -K_2\Delta_{BL}H$. In this case, our usual division of the solution gives the very simple expression for the deterministic radial part $R(t) = Ft$, while the stochastic perturbation can be expressed as an infinite series of spherical harmonics. For the different modes we get the equation

$$\frac{d\rho_l^m}{dt} = -\frac{K_2}{F^4t^4}[l(l+1)(l^2+l+2)]\rho_l^m + \frac{\eta_l^m(t)}{Ft}, \tag{52}$$

and so for the mean value we obtain

$$\langle\rho_l^m(t)\rangle = \exp\left[\frac{K_2[l(l+1)(l^2+l+2)]}{3F^4}(t^{-3}-t_0^{-3})\right]\langle\rho_l^m(t_0)\rangle\,, \tag{53}$$

what reveals that all the modes are stable, but $l = 0$ that is marginal. For the correlation we get

$$\begin{aligned} C_{l,l'}^{m,m'}(t) = \exp\left(\frac{K_2}{3F^4}[l(l+1)(l^2+l+2)+l'(l'+1)(l'^2+l'+2)(t^{-3}-t_0^{-3})]\right)\times \\ C_{l,l'}^{m,m'}(t_0) + \frac{(-1)^m}{3F^2}\exp\left(\frac{K_2}{3F^4t^3}[l(l+1)(l^2+l+2)+l'(l'+1)(l'^2+l'+2)]\right)\times \\ \delta_{m,-m'}\delta_{l,l'}\left\{t^{-1}\varphi_{-2/3}\left(\frac{K_2}{3F^4t^3}[l(l+1)(l^2+l+2)+l'(l'+1)(l'^2+l'+2)]\right)\right. \\ \left. -t_0^{-1}\varphi_{-2/3}\left(\frac{K_2}{3F^4t_0^3}[l(l+1)(l^2+l+2)+l'(l'+1)(l'^2+l'+2)]\right)\right\}, \end{aligned} \tag{54}$$

where $\varphi_n(x) = \int_1^\infty y^n e^{-xy}dy$ is the Misra function [36]. Using the expansion $\varphi_{-2/3}(x) \sim \Gamma(1/3)x^{-1/3}$ (here $\Gamma(x)$ denotes the gamma function and $\Gamma(1/3) \approx 2.68$) when $x \sim 0$ we see that the correlation is bounded in the infinite time limit and that we recover the same result, Eq.(45), as in the other two spherical cases.

IV. OTHER GEOMETRIES

It is also interesting, both at the theoretical and applied levels, to consider geometries that do not preserve the spherical symmetry. The simplest case might be elliptic geometry, see Fig. 3. An example of elliptic interface is provided by epithelial cell populations on stretched elastic substrates [9]. We will consider the position vector

$$\vec{r} = (r(\theta,t)\cos(\theta), ar(\theta,t)\sin(\theta)), \tag{55}$$

where $a > 1$ is some parameter specifying the ellipse eccentricity. Following the techniques developed in [21], we can derive the EW equation in elliptic geometry. However, as could

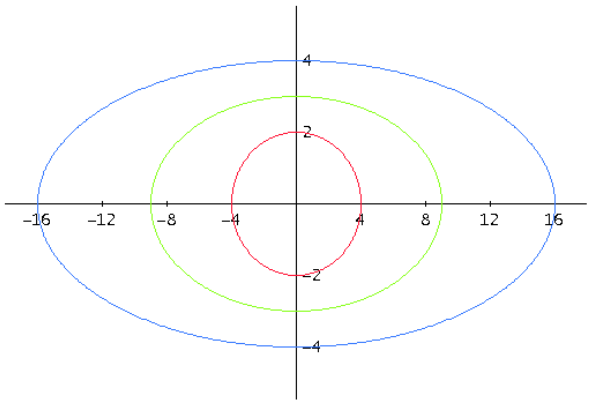


FIG. 3: Sketch of a deterministically growing elliptic interface of constant eccentricity. Red (inner) line, short times; green (middle) line, intermediate times; blue (outer) line, long times. Stochasticity will manifest itself as small Gaussian fluctuations about the deterministic shape in the small noise approximation.

be expected, the resulting equation is not spatially homogeneous, as it explicitly depends on the angle θ. As an example, we show the expression of the metric tensor (note that, due to the low dimensionality, the metric tensor is a scalar in this case), keeping only the terms that are linear in the derivatives of the radius

$$g = a^2 r^2 \cos^2(\theta) + r^2 \sin^2(\theta) + (a^2 - 1) r r_\theta \sin(2\theta). \tag{56}$$

For the sake of simplicity, we will derive two EW equations, one that locally describes the points that are equidistant to the ellipse foci, which is

$$\partial_t r = \frac{D}{a^2}\left(\frac{\partial_\theta^2 r}{r^2} - \frac{1}{r}\right) + F + \frac{1}{\sqrt{ar}}\xi(\theta, t), \tag{57}$$

and the other one for the points that lie the closest to one of the foci

$$\partial_t r = D\left(\frac{\partial_\theta^2 r}{r^2} - \frac{1}{r}\right) + \frac{F}{a} + \frac{1}{a\sqrt{r}}\xi(\theta, t). \tag{58}$$

The advantage of these concrete points is that they are the only ones affected by isotropic growth. As can be seen, the growth is qualitatively identical to that of the radial cluster. At the quantitative level, one can see that the neighborhood of the minor axis is affected by a reduced diffusion, while the neighborhood of the major axis is affected by reduced growth and fluctuations. Let us now consider the random deposition model in ellipsoidal geometry

$$\vec{r} = (ar(\theta, \phi, t)\cos(\phi)\sin(\theta), r(\theta, \phi, t)\sin(\theta)\sin(\phi), r(\theta, \phi, t)\cos(\theta)); \tag{59}$$

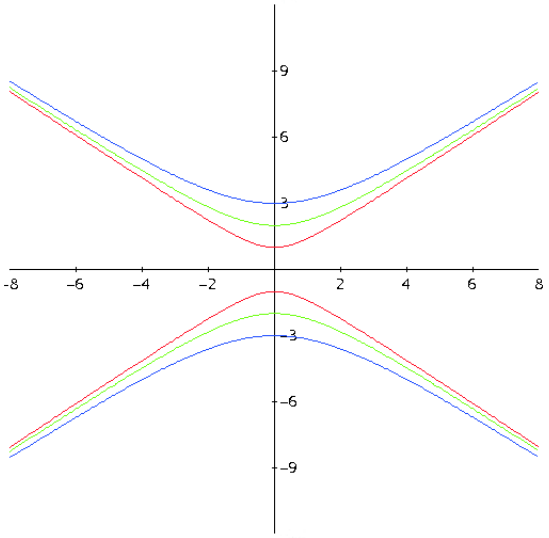


FIG. 4: Sketch of a deterministically growing hyperbolic interface of $\sqrt{2}$ eccentricity. Red (inner) line, short times; green (middle) line, intermediate times; blue (outer) line, long times. Stochasticity will manifest itself as small Gaussian fluctuations about the deterministic shape in the small noise approximation.

we will concentrate on the dynamics on the $\theta = \pi/2$ plane. The ellipse lying on this plane is similar to the one just described above but the random deposition model reads in this case

$$\partial_t r = \frac{F}{a} + \frac{1}{ar}\xi(\theta, \phi, t), \tag{60}$$

near the major axis, and

$$\partial_t r = F + \frac{1}{r\sqrt{a}}\xi(\theta, \phi, t), \tag{61}$$

near the minor axis, where $\xi(\theta, \phi, t)$ is a zero mean Gaussian noise whose correlation is given by

$$\langle \xi(\theta, \phi, t)\xi(\theta', \phi', t')\rangle = \epsilon\delta(\theta - \theta')\delta(\phi - \phi')\delta(t - t'). \tag{62}$$

Like in the $1 + 1d$ case the neighborhood of the major axis is affected by reduced growth rate and fluctuations intensity, while the neighborhood of the minor axis undergoes a smaller reduction of the fluctuations intensity but its growth rate remains unchanged. As in the spherical case, the strong negative power of the radius in the noise term will cause a constant average roughness that depends on the perturbation initial time.

The opposite case to elliptic geometry is hyperbolic geometry, see Fig. 4. This geometry could perhaps be useful in describing atomic ledges bordering crystalline facets [5]. In this case, different layers in the solid corner would correspond to the different hyperbolas. If we define the position vector as

$$\vec{r} = (\rho(\chi, t)\sinh(\chi), \rho(\chi, t)\cosh(\chi)), \tag{63}$$

then $\rho \geq 0$ is the "radius" of the hyperbola upper branch, to which we will limit our study, and $\chi \in \mathbb{R}$ is the hyperbolic angle. This geometry is again characterized by a nonhomogeneous growth equation, so we will focus on the hyperbola vertex in order to obtain an isotropic result. In this case the resulting EW equation reads

$$\partial_t \rho = D\left(\frac{\partial_\chi^2 \rho}{\rho^2} + \frac{1}{\rho}\right) + F + \frac{1}{\sqrt{\rho}}\xi(\chi, t). \tag{64}$$

Performing as usual the expansion $\rho(\chi, t) = \mathcal{R}(t) + \epsilon\sigma(\chi, t)$, where ϵ is the small noise amplitude, we get the zeroth order equation

$$\frac{d\mathcal{R}}{dt} = F + \frac{D}{\mathcal{R}}, \tag{65}$$

that can be solved to yield

$$\mathcal{R}(t) = -\frac{D}{F}\left\{1 + \mathcal{W}_{-1}\left(-\frac{D + F\mathcal{R}_0}{D}\exp\left[-\frac{D + F(\mathcal{R}_0 + Ft)}{D}\right]\right)\right\}, \tag{66}$$

where $\mathcal{W}_{-1}$ is the corresponding branch of the Lambert omega function [29], and $\mathcal{R}_0 = \mathcal{R}(0)$. One can read from this equation that the growth is faster than linear, but it evolves towards the linear law $\mathcal{R}(t) \sim Ft$ in the long time limit, see Fig. 5. Furthermore, there are no fixed points in the dynamics, and the system can only expand, and not shrink like in the radial case. The equation for the perturbation is

$$\partial_t \sigma = D\left(\frac{\partial_\chi^2 \sigma}{\mathcal{R}(t)} - \frac{\sigma}{\mathcal{R}(t)}\right) + \frac{\eta}{\mathcal{R}(t)}, \tag{67}$$

where as usual η is a zero mean Gaussian noise which correlation is given by

$$\langle \eta(\chi, t)\eta(\chi', t')\rangle = \epsilon\delta(\chi - \chi')\delta(t - t'). \tag{68}$$

Now one sees that, contrary to the radial case, all the terms in the drift of the equation for the perturbation are stabilizing, and even a homogeneous perturbation decreases in time

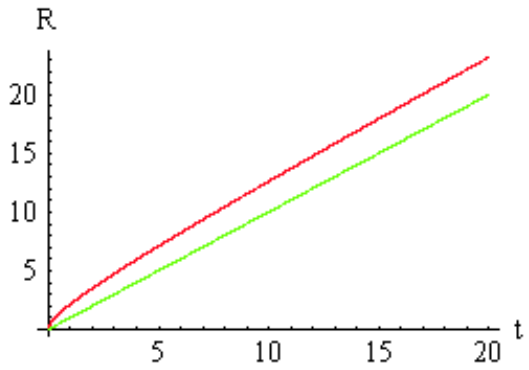


FIG. 5: Deterministic growth of the hyperbolic interface at zeroth order in the small noise expansion, see Eq. (66) in the main text, with parameter values $F = 1$, $D = 1$, and $\mathcal{R}_0 = 10^{-4}$ (red upper line). The linear law $t + 10^{-4}$ is plotted for comparison (green lower line).

due to their action. To study the higher dimensional growth properties of a hyperbolic surface let us now consider a double sheeted revolution hyperboloid. The upper sheet may be parameterized with the vector

$$\vec{r} = (\rho(\chi, \phi, t)\sinh(\chi)\cos(\phi), \rho(\chi, \phi, t)\sinh(\chi)\sin(\phi), \rho(\chi, \phi, t)\cosh(\chi)), \tag{69}$$

and the random deposition model, next to the vertex, reads in this case

$$\partial_t \rho = F + \frac{1}{\rho\sqrt{|\chi|}}\xi(\chi, \phi, t), \tag{70}$$

what reveals that the hyperbolic surface develops a constant average roughness in this case as well, just like the spherical and ellipsoidal geometries. Note that the vertex of the hyperboloid, parameterized as $\chi = 0$, is a singular point characterized by an infinite amplitude of the fluctuations. This paradox is solved by taking into account nonlinear terms in the derivatives of the field

$$\partial_t \rho = F + \frac{1}{\sqrt[4]{\chi^2\rho^4 + \rho^2\rho_\phi^2}}\xi(\chi, \phi, t). \tag{71}$$

Finally, another interesting geometry is that of a growing parabolic surface, see Fig. 6. Stromatolite morphogenesis might be related to parabolic geometry, as has been pinpointed in recent works [30, 31]. Using the parameterization

$$\vec{r} = (2x\Phi(x, t), (1 - x^2)\Phi(x, t)), \tag{72}$$

where $x \in \mathbb{R}$ and $\Phi \geq 0$, we obtain the EW equation

$$\partial_t \Phi = D\left(\frac{\partial_x^2 \Phi}{4\Phi^2} - \frac{1}{2\Phi}\right) + F + \frac{1}{\sqrt{2\Phi}}\xi(x,t), \tag{73}$$

for the dynamics close to the vertex of the parabola, $x = 0$, the only point where isotropy holds. The noise ξ is Gaussian and zero centered, and its correlation is given by

$$\langle \xi(x,t)\xi(x',t')\rangle = \epsilon\delta(x-x')\delta(t-t'). \tag{74}$$

One can see that this equation describes a dynamics which is identical to the spherical one, up to some numerical adjustment. The paraboloidal geometry can be characterized by the position vector

$$\vec{r} = (2x\Phi(x,\phi,t)\cos(\phi), 2x\Phi(x,\phi,t)\sin(\phi), (1-x^2)\Phi(x,\phi,t)), \tag{75}$$

that rends a random deposition model

$$\partial_t \Phi = F + \frac{1}{2\Phi\sqrt{|x|}}\xi(x,\phi,t), \tag{76}$$

where the zero centered Gaussian noise is again delta correlated and has some intensity ϵ. As in the hyperbolic case, the noise produces an average constant roughness depending on the perturbation initial time, and the vertex is again a singular point. Taking into account the lowest order nonlinearity in the vertex the resulting equation is

$$\partial_t \Phi = F + \frac{1}{\sqrt[4]{16x^2\Phi^4 + 4\Phi^2\Phi_\phi^2}}\xi(x,\phi,t). \tag{77}$$

As can be seen, parabolic interfacial dynamics lies between the elliptic and hyperbolic cases. This is rather natural, as a parabola is the conical curve that represents the marginal situation between the ellipse and the hyperbola.

V. CONCLUSIONS

The dynamics of radially symmetric surfaces has been studied in sections II and III. In Sec. III we have calculated for the first time the explicit correlations of the spherical models, and we have shown that the long time average roughness becomes constant in polar coordinates, but at the same time it develops memory with respect to the initial conditions. In

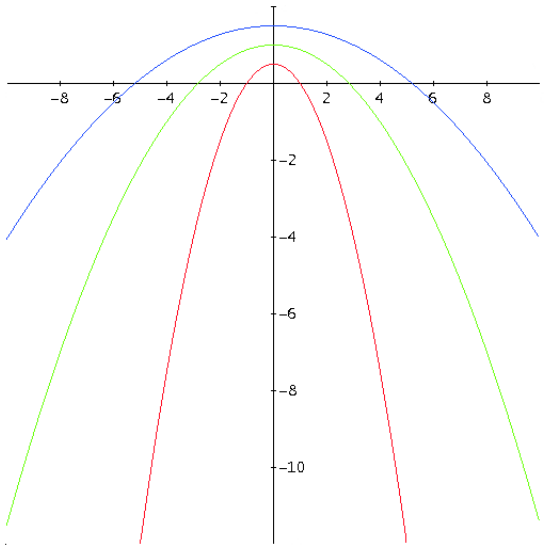


FIG. 6: Sketch of a deterministically growing parabolic interface. Red (lower) line, short times; green (middle) line, intermediate times; blue (upper) line, long times. Stochasticity will manifest itself as small Gaussian fluctuations about the deterministic shape in the small noise approximation.

Sec. II it is shown also for the first time that sub-ballistic diffusion radial models reduce to radial random deposition in the long time limit and for large angular scales. Radial random deposition is characterized by an uncorrelated interface of a logarithmic temporal amplitude, as was shown in [23]. The model with ballistic correlations propagation, introduced here in radial geometry, shows a richer phenomenology. Despite the logarithmic temporal dependence, the correlation function is markedly different. In fact, the analysis of this function for long times and short angular scales reveals the appearance of a local dynamical exponent z_{loc}, which is equal to the ratio of the constant rate of radius growth F and the ballistic diffusion constant D_1, and it is thus nonuniversal. This reflects the fact that the microscopic details of the growth process influence the surface scaling at the local level. We have also shown for the first time that our results in radially symmetric geometries seem to be metric independent. We have been able to reproduce them in elliptic, hyperbolic, and parabolic geometries, which undergo particular nonlinear effects, but share the same stochastic dynamics. The differences among the classical results on surface growth and the current ones are related to the substrate growth properties. The classical setting assumes a constant d dimensional substrate size, and growth is restricted to the $(d+1)$th spatial

dimension. In the parameterizations we have considered here, growth happens equally in every spatial dimension, a fact that has been ensured by keeping constant the eccentricity of the different underlying conical structures. Indeed, in Sec. IV we have kept the eccentricity constant explicitly by means of the introduction of the parameter a. In this same section, hyperbolic geometry has been implicitly supposed of $\sqrt{2}$ eccentricity, but assuming an arbitrary constant eccentricity would yield a straightforward modification of these results, just along the lines of the elliptic case, and it would rend the stochastic dynamics unchanged. A different situation might arise if the eccentricity changes along the evolution. For instance, consider an ellipsoid growing in all spatial dimensions at different rates. Its shape will change in time, and this might affect the surface dynamics. In this case, different spatio-temporal scales will enter in competition, and the resulting growth dynamics might combine features of the different scenarios studied so far and perhaps new ones. In any case, due to the complex nature of these growth regimes, it is necessary to build some analytical progress before drawing any conclusions about them.

A necessary step in the following is the study of the relationship among stochastic growth equations and discrete models. On the applied side, important technological processes such as liquid composite molding [11] are driven by growing radial interfaces. The theoretical study of this sort of systems is often based on detailed numerical simulations, which could be simplified using eikonal descriptions like the stochastic growth equations presented here. The duality expansion versus shrinking present in the radial and spherical EW equations and IS equation might be related to some of the observed phenomena. Interface shrinking is present in adatom islands, which can disappear if they are composed of a subcritical number of particles [32]. The comparison with numerical simulations and experiments will facilitate a deeper understanding of the dynamics of curved surfaces.

Acknowledgments

This work has been partially supported by the Ministerio de Educación y Ciencia (Spain) through Project No. FIS2005-01729.

APPENDIX A: ESTIMATING THE EFFECT OF EXPONENTIALLY INFREQUENT EVENTS

In this appendix we will estimate the effect of rare events on the evolution of the radial random deposition process using large deviation theory. This process is described by the radial EW equation after setting $D = 0$ [23]. The equation of motion in the one dimensional case reads

$$\partial_t r = F + r^{-1/2}\eta(\theta, t), \tag{A1}$$

that is actually a stochastic ordinary differential equation. The noise correlation is given by

$$\langle \eta(\theta, t)\eta(\theta', t')\rangle = \epsilon\delta(\theta - \theta')\delta(t - t'). \tag{A2}$$

We will assume the following form of the probability distribution (which is in fact a WKB ansatz)

$$P(r, t) = \exp[\Phi(r, t)/\epsilon], \tag{A3}$$

and in the limit of vanishing noise intensity $\epsilon \to 0$ we find

$$\partial_t \Phi = -F\partial_r \Phi + \frac{(\partial_r \Phi)^2}{2r}. \tag{A4}$$

The equation for its derivative $\Psi = \partial_r \Phi$ can be solved along characteristics

$$\frac{d\Psi}{dt} = -\frac{\Psi^2}{2r^2}, \tag{A5}$$

$$\frac{dr}{dt} = F - \frac{\Psi}{r}. \tag{A6}$$

The analysis of the characteristic equations show the temporal behavior of the radius

$$r(t) \approx Ft + \frac{\psi_0}{F}\ln(Ft), \tag{A7}$$

in the long time limit, where $\psi_0 = \Psi(0)$ measures the initial size of the rare fluctuation, and we have assumed that $Fr(0) \gg |\psi_0|$. This result shows that the effect of these exponentially infrequent events is negligible in the long time limit. Redoing this same analysis for $d > 1$ one finds that the logarithmic correction is substituted by a constant proportional to ψ_0, what shows that the effect of rare fluctuations is even weaker in this case. This analysis totally agrees with the results obtained from the small noise expansions in Sec. II and III.

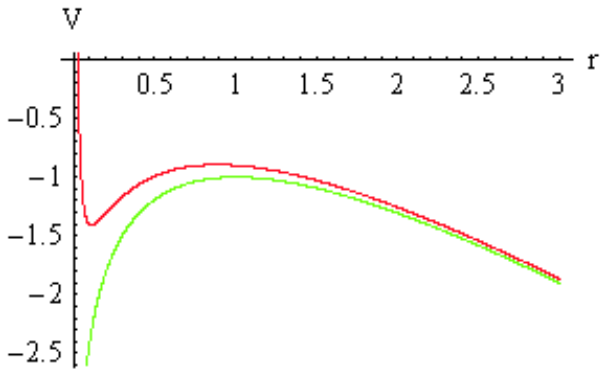


FIG. 7: Deterministic (green lower line) and effective stochastic potential (red upper line) for the mean-field model of the radial EW equation. The parameter values are $F = 1$, $D = 1$, and $\epsilon = 0.4$.

APPENDIX B: METASTABILITY IN THE RADIAL EDWARDS-WILKINSON EQUATION

In Ref. [16] the authors investigate the behavior of the interface driven by the radial EW equation. To this end, they use the Itô stochastic differential equation

$$\frac{dr}{dt} = F - \frac{D}{r} + \frac{1}{\sqrt{r}}\xi(t), \tag{B1}$$

$$\langle \xi(t)\xi(t')\rangle = \epsilon\delta(t-t'), \tag{B2}$$

as a mean field model, and they showed that it represents well the dynamics of a lattice simulation interface. The deterministic fixed point is given by $r_c = D/F$, that separates the shrinking and growing phases. However, the presence of the noise term can alter this scenario. We can interpret Eq. (B1) as the overdamped description of a particle moving on the singular potential $\mathcal{V}(r) = D\ln(r) - Fr$, that possesses two wells of infinite depth, the origin and the positive infinity, and it is subject to state-dependent noise. We can calculate the mean time that it takes this particle to leave the well at the origin, and to roll down to infinity after overcoming the maximum at r_c. It is given by the solution to the well known equation [24]

$$\frac{\epsilon}{2r}T'' + \left(F - \frac{D}{r}\right)T' = -1, \tag{B3}$$

where $T = T(r)$ is the mean time at which a particle starting at r, $0 \leq r \leq r_c$, reaches the position r_c, and thus, the mean first passage time can be defined as $2T$. The correct boundary condition at r_c is an absorbing one $T(r_c) = 0$. At the origin we will assume we

have a reflecting boundary $T_r(0) = 0$, a fact that we will explain in more detail below. The solution of this equation subject to the mentioned boundary conditions can be readily computed, but for simplicity we will only state the result for an initial condition at the origin $T_0 = \lim_{r\to 0} T(r)$

$$\frac{F^2}{D}T_0 = 1 + \frac{1}{2}\mathrm{erf}(x)\left[\pi \mathrm{erfi}(x) - \frac{\sqrt{\pi}}{x}e^{x^2}\right] - {}_2F_2(1,1;3/2,2;-x^2)x^2, \tag{B4}$$

where $x = D/\sqrt{\epsilon F}$, $\mathrm{erf}(z) = 2\pi^{-1/2}\int_0^z e^{-y^2}dy$ is the error function [27], $\mathrm{erfi}(z) = -i\mathrm{erf}(iz)$ is the imaginary error function, and ${}_2F_2(a_1,a_2;b_1,b_2;z)$ is the corresponding generalized hypergeometric function [33]. Of course, if we solve the passage problem for an initial condition such that $r_c < r < +\infty$, the mean first passage time is always divergent.

Despite its exactness, this formula is very complex, and a further clarification of the passage process is in order. To accomplish this, we can use the Stratonovich version of Eq. (B1)

$$\frac{dr}{dt} = F - \frac{D}{r} + \frac{\epsilon}{4r^2} + \frac{1}{\sqrt{r}} \circ \xi(t), \tag{B5}$$

and by changing variables $u = r^{3/2}$ we obtain the additive noise equation

$$\frac{2}{3}\frac{du}{dt} = Fu^{1/3} - Du^{-1/3} + \frac{\epsilon}{4}u^{-1} + \xi(t) = -\frac{2}{3}\mathcal{V}_u'(u) + \xi(t), \tag{B6}$$

where the new potential is defined as

$$\frac{8}{3}\mathcal{V}_u(u) = -6Du^{2/3} + 3Fu^{4/3} + \epsilon\ln(u). \tag{B7}$$

The evolution of the probability functional associated to the random variable $u(t)$ can be cast in the form of a path integral [34] which action reads

$$S[u(t)] = \frac{2}{9}\int_{-\infty}^{\infty}\left\{\dot{u}(t) + \mathcal{V}_u'[u(t)]\right\}^2 dt. \tag{B8}$$

Its first variation $\delta S/\delta u = 0$ gives the equation for the classical trajectory

$$\ddot{u} = \mathcal{V}_u'\mathcal{V}_u'', \tag{B9}$$

that admits a first integral of motion, and using the fact that the particle stops at either the minimum or the maximum of the potential, we conclude that the integration constant is zero. We are thus led to the equation

$$\dot{u}^2 = \mathcal{V}_u'(u)^2. \tag{B10}$$

Taking the square root we find

$$\frac{2}{3}\frac{du}{dt} = Fu^{1/3} - Du^{-1/3} + \frac{\epsilon}{4}u^{-1}, \tag{B11}$$

where we have selected the negative square root. The positive square root is the instanton solution that indicates the optimal path for escaping from the potential well [34]. Re-changing variables to recover the description in terms of r we find

$$\frac{dr}{dt} = F - \frac{D}{r} + \frac{\epsilon}{4r^2}, \tag{B12}$$

which is nothing but the Stratonovich equation (B5) with the noise term suppressed [35]. The mean field equation (B12) represents motion on the effective potential

$$\mathcal{V}_e = D\ln(r) - Fr + \frac{\epsilon}{4r}, \tag{B13}$$

which is positively divergent at the origin, justifying the choice of a reflecting boundary at the origin earlier in Eq. (B3). This effective potential is a regularized version of the corresponding one in Eq. (B1), and it has a finite depth minimum at $r_{min} = (2F)^{-1}(D - \sqrt{D^2 - \epsilon F})$, and a finite height maximum at $r_{max} = (2F)^{-1}(D + \sqrt{D^2 - \epsilon F})$, provided $D^2 > \epsilon F$. Otherwise it is monotonically decreasing in r, implying the loss of metastability. So we see that the simple picture of bistability drawn by the small noise expansion can be modified due to the divergent amplitude of the fluctuations at the origin. However, the behavior for long r remains the same. A comparison between both potentials can be found in Fig. 7.

For the bistable spherical models EW and IS we can derive the same kind of mean field equations

$$\frac{dr}{dt} = F - \frac{2K_0}{r} + \frac{1}{r}\xi(t), \tag{B14}$$

$$\frac{dr}{dt} = F - \frac{K_1}{r^2} + \frac{1}{r}\xi(t), \tag{B15}$$

respectively, and the corresponding semiclassical description

$$\frac{dr}{dt} = F - \frac{2K_0}{r} + \frac{\epsilon}{2r^3}, \tag{B16}$$

$$\frac{dr}{dt} = F - \frac{K_1}{r^2} + \frac{\epsilon}{2r^3}. \tag{B17}$$

In both cases we find the same regularization as for the radial EW equation, because we know, by applying Descartes rule, that in the stationary regime these last two equations

have either none or two roots. The exact values of the maximum and the minimum of the potential, and the threshold condition for the existence of bistability are again within reach, since any cubic polynomial equation can be solved in terms of radicals. However, as usually happens, the solutions are cumbersome and not particularly illuminating, and so we will omit the exact expressions here. Of particular interest is Eq. (32), which mean field model reads

$$\frac{dr}{dt} = F - \frac{K_0}{r} + \frac{K_2}{r^3} + \frac{1}{\sqrt{r}}\xi(t). \tag{B18}$$

In this case, suppressing the noise term either in the Itô or the Stratonovich interpretation yields the same qualitative behavior of the effective potential. This shows that the deterministic evolution of this equation is more robust to stochastic perturbations, and suggests that the type of equations that can be obtained from series like (30) might be a good starting point for modelling the growth of complex interfaces with general geometric symmetries.

APPENDIX C: THE PLANAR BALLISTIC MODEL

The ballistic model in planar geometry reads

$$\partial_t h = D_1 \Lambda h + \xi(x,t), \tag{C1}$$

and its Fourier transform is

$$\partial_t \hat{h} = -D_1|k|\hat{h} + \hat{h}(k,t), \tag{C2}$$

that can be solved to yield

$$\hat{h}(k,t) = \int_{-\infty}^{\infty} e^{D_1|k|(s-t)}\hat{\xi}(k,s)ds. \tag{C3}$$

The correlation in Fourier space reads

$$\left\langle \hat{h}(k,t)\hat{h}(q,t)\right\rangle = \epsilon \int_0^t e^{D_1(|k|+|q|)(s-t)}\delta(k+q)ds, \tag{C4}$$

and in real space

$$\langle h(x,t)h(y,t)\rangle = \epsilon \int_{-\infty}^{\infty} dk \int_{-\infty}^{\infty} dq \int_0^t ds \left[e^{i(kx+qy)}e^{D_1(|k|+|q|)(s-t)}\delta(k+q)\right] = \frac{\epsilon}{2D_1}\ln\left(1+\frac{4D_1^2t^2}{|x-y|^2}\right) \to \frac{\epsilon}{D_1}\ln\left(\frac{t}{|x-y|}\right), \tag{C5}$$

when $t \to \infty$. As a final note, let us remark that this simple analysis has been made in order to obtain a comparison with the results in section II. A more detailed analysis can be found in [25].

---

[1] A.-L. Barabási and H. E. Stanley, *Fractal Concepts in Surface Growth*, (Cambridge University Press, Cambridge, 1995).

[2] S. F. Pinto, M. S. Couto, A. P. F. Atman, S. G. Alves, A. T. Bernardes, H. F. V. de Resende, and E. C. Souza, Phys. Rev. Lett. **99**, 068001 (2007).

[3] B. B. Mandelbrot, D. E. Passoja, and A. J. Paullay, Nature (London) **308**, 721 (1984).

[4] S. V. Khare and T. L. Einstein, Phys. Rev. B **54**, 11752 (1996).

[5] P. L. Ferrari, M. Prähofer, and H. Spohn, Phys. Rev. E **69**, 035102(R) (2004).

[6] M. Degawa, T. J. Stasevich, W. G. Cullen, A. Pimpinelli, T. L. Einstein, and E. D. Williams, Phys. Rev. Lett. **97**, 080601 (2006).

[7] E. Ben-Jacob, I. Cohen, and H. Levine, Adv. Phys. **49**, 395 (2000).

[8] S. Matsuura and S. Miyazima, Physica A **191**, 30 (1992).

[9] J. Galle, M. Loeffler, and D. Drasdo, Biophys. J. **88**, 62 (2005).

[10] R. Messier and J. E. Yehoda, J. Appl. Phys. **58**, 3739 (1985).

[11] F. Sánchez, J. A. García, F. Chinesta, L. I. Gascón, C. Zhang, Z. Liang, and B. Wang, Compos. Part A: Appl. Sci. Manuf. **37**, 903 (2006).

[12] M. T. Batchelor, R. V. Burne, B. I. Henry, and S. D. Watt, Math. Geology **35**, 789 (2003).

[13] V. I. Roldughin, Uspekhi Khimii **72**, 931 (2003).

[14] M. Eden, in *Symposium on Information Theory in Biology*, edited by H. P. Yockey (Pergamon, New York, 1985).

[15] A. Maritan, F. Toigo, J. Koplik, and J. R. Banavar, Phys. Rev. Lett. **69**, 3193 (1992).

[16] R. Kapral, R. Livi, G.-L. Oppo, and A. Politi, Phys. Rev. E **49**, 2009 (1994).

[17] M. T. Batchelor, B. I. Henry, and S. D. Watts, Physica A **260**, 11 (1998).

[18] S. B. Singha, J. Stat. Mech.: Theory Exp. P08006 (2005).

[19] C. Escudero, Phys. Rev. E **73**, 020902(R) (2006).

[20] C. Escudero, Phys. Rev. E **74**, 021901 (2006).

[21] M. Marsili, A. Maritan, F. Toigo, and J. R. Banavar, Rev. Mod. Phys. **68**, 963 (1996).

[22] C. Escudero, J. Stat. Mech.: Theor. Exp. (in press), arXiv:0901.2733.

[23] C. Escudero, Phys. Rev. Lett. **100**, 116101 (2008).

[24] C. W. Gardiner, *Handbook of Stochastic Methods* (Springer-Verlag, Berlin, 1996).

[25] A. Röthlein, F. Baumann, and M. Pleimling, Phys. Rev. E **74**, 061604 (2006).

[26] R. Metzler and J. Klafter, Phys. Rep. **339**, 1 (2000).

[27] M. Abramowitz and I. A. Stegun (editors), *Handbook of Mathematical Functions with Formulas, Graphs, and Mathematical Tables* (Dover, New York, 1972).

[28] E. E. Gruber, J. Appl. Phys. **38**, 243 (1967).

[29] R. M. Corless, G. H. Gonnet, D. E. G. Hare, D. J. Jeffrey, and D. E. Knuth, Adv. Comput. Math. **5**, 329 (1996).

[30] M. T. Batchelor, R. V. Burne, B. I. Henry, and M. J. Jackson, Physica A **337**, 319 (2004).

[31] M. T. Batchelor, R. V. Burne, B. I. Henry, and T. Slatyer, Physica A **350**, 6 (2005).

[32] A. Pimpinelli and T. L. Einstein, Phys. Rev. Lett. **99**, 226102 (2007).

[33] B. Dwork, *Generalized Hypergeometric Functions* (Oxford University Press, Oxford, 1990).

[34] A. J. Bray and A. J. McKane, Phys. Rev. Lett. **62**, 493 (1989).

[35] V. E. Shapiro, Phys. Rev. E **48**, 109 (1993).

[36] R. D. Misra, Proc. Cambridge Phil. Soc. **36**, 173 (1940).